



UNIVERSITY OF LEEDS

This is a repository copy of *Compliance control for stabilizing the humanoid on the changing slope based on terrain inclination estimation*.

White Rose Research Online URL for this paper:
<http://eprints.whiterose.ac.uk/144471/>

Version: Accepted Version

Article:

Li, Z, Zhou, C orcid.org/0000-0002-6677-0855, Tsagarakis, N et al. (1 more author) (2016) Compliance control for stabilizing the humanoid on the changing slope based on terrain inclination estimation. *Autonomous Robots*, 40 (6). pp. 955-971. ISSN 0929-5593

<https://doi.org/10.1007/s10514-015-9504-6>

© Springer Science+Business Media New York 2015. This is a post-peer-review, pre-copyedit version of an article published in *Autonomous Robots*. The final authenticated version is available online: <https://doi.org/10.1007/s10514-015-9504-6>.

Reuse

Items deposited in White Rose Research Online are protected by copyright, with all rights reserved unless indicated otherwise. They may be downloaded and/or printed for private study, or other acts as permitted by national copyright laws. The publisher or other rights holders may allow further reproduction and re-use of the full text version. This is indicated by the licence information on the White Rose Research Online record for the item.

Takedown

If you consider content in White Rose Research Online to be in breach of UK law, please notify us by emailing eprints@whiterose.ac.uk including the URL of the record and the reason for the withdrawal request.



eprints@whiterose.ac.uk
<https://eprints.whiterose.ac.uk/>

Compliance Control for Stabilizing the Humanoid on the Changing Slope Based on Terrain Inclination Estimation

Zhibin Li, Chengxu Zhou, Nikos Tsagarakis, Darwin Caldwell

September, 2015. *This is a draft version, please find official version by DOI:10.1007/s10514-015-9504-6*

Abstract This paper presents a stabilization framework integrated with the estimation of the terrain inclination to balance a humanoid on the changing slope as an extension to our previous study [9]. In this paper, the estimation of the terrain inclination is improved for walking in place on an inclination-varying slope. A passivity based admittance control utilizes the force/torque sensing in feet to actively regulate the impedance at the center of mass to stabilize the robot. The logic-based inclination estimation algorithm uses the feet to probe the terrain and deals with the under-actuation. The equilibrium set-point in the admittance control is regulated based on the detected inclination. The effectiveness of the control framework is validated on the humanoid robot COMAN and demonstrated by estimating the terrain inclination, coping with the under-actuation phase, adapting to the slope with changing inclination during both standing and walking. Experimental data are analyzed and discussed, and the future work is suggested.

Keywords Stabilization; Compliance Control; Admittance Control

1 Introduction

Humanoids that interact in an uncertain environment demand compliance at the contact interface to maintain

Zhibin Li, Chengxu Zhou, Nikos Tsagarakis, Darwin Caldwell
Department of Advanced Robotics, Istituto Italiano di Tecnologia, via Morego, 30, 16163 Genova, Italy
Tel.: +39-010-71781865
Fax: +39-010-71781232
E-mail: alexrobotics@gmail.com; zhibin.li@iit.it
E-mail: chengxu.zhou@iit.it
E-mail: nikos.tsagarakis@iit.it
E-mail: darwin.caldwell@iit.it

stable interactions. Compliance can mitigate collision forces, dissipate undesired energy, and thereby warrant stable execution of tasks [3]. Meanwhile, the accompanied passivity property of compliance is essential for both manipulators with immovable bases [13] [1] and walking robots [4] [5] to be self-stable.

The compliant property can be exploited for balancing the humanoids because the robot with compliance naturally deforms under external forces, therefore the magnitude of impacts is reduced. This allows more time for the robot to react and attenuate undesired energy delivered by the disturbances. The compliant behavior can be realized through different control paradigms based on impedance or admittance schemes. The realization using the impedance control approach requires a system to have fully torque controlled actuators such as the Sarcos humanoid [5], [19], and the DLR-biped [14], [15]. For the balance recovery, the common ground of these torque control based works is the use of Cartesian impedance control at the center of mass (COM), which generates desired wrench and distributes contact forces over the support polygon by controlling the joint torque tracking.

The admittance based scheme implements compliance control for the systems with position controlled actuators and force/torque sensors at the end-effectors. The past works demonstrated the effectiveness of compliance particularly for absorbing landing impacts and adapting terrain inclination. Kim et. al [6] proposed PI control to superimpose an angular compensation of the ankle joint using excessively filtered inclination error measured from the torso of the robot. The method aimed at handling slow variation of the floor inclination, but how to deal with the foot titling was not yet discussed. On the WL-16R biped locomotor, Sugahara et al. used foot compliance control to decrease the landing

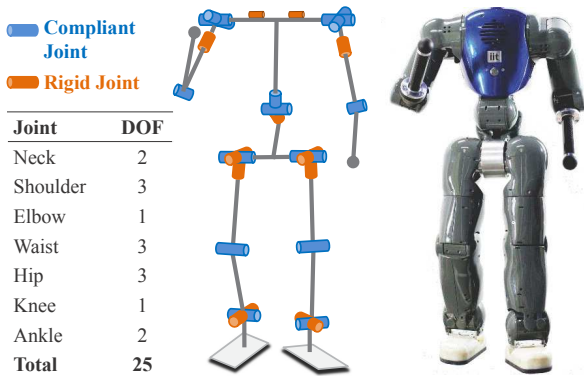


Fig. 1 The compliant humanoid robot COMAN.

impact, and applied PD control with normalized gains to compute the translational and angular acceleration of the waist in order to generate the positional compensation [21]. Their experiments demonstrated successful adaptation to a surface with a constant inclination up to 8° . However, it was not shown further if the method could adapt to a changing slope. Hashimoto et al. proposed predictive attitude control for WL-16RII robot, which integrated zero moment point (ZMP) errors to compute the compensation for the pitch and roll angles [2]. The integral control was only applied for a fixed time window and reset at each footstep.

Heuristic methods inspired by humans [11] [17], such as the ankle and hip strategies, were introduced as a bio-inspired approach for the stance balancing control. The work in [12] used virtual models to synthesize the ankle and hip strategies. Other engineering techniques such as linear quadratic regulator (LQR) and integral control were also introduced to resemble the ankle and hip strategies [18].

To the best of our knowledge, the above works presumed that the feet of the robot were always firmly flat on the ground, and dealing with the under-actuation during foot tilting was not discussed. This problem was overlooked in the past, most probably because the external push applied by the human operator was insufficient to create the under-actuation for these adult-size humanoids. The scope of our paper focuses on the cases where the disturbance is large enough to create under-actuation phase but not yet to completely tip over the robot. For the cases out of our scope, where the disturbance is extremely large to topple the robot from the standing posture, other strategies, such as the stepping strategy, shall be adopted [20] [7] [16].

The novel contribution of this paper is a new stabilization framework for balancing humanoids in the stance posture under medium perturbations. It consists of:

Table 1 Parameters used in the admittance control

m :	mass of the system
l :	nominal pendulum length from COM to pivot
I_c :	inertia tensor around COM
I :	inertia tensor around pivot $I = I_c + ml^2$
θ_d :	desired motor position reference
θ_s :	angular deflexion due to resultant elasticity
q_0 :	the equilibrium position of the pendulum
q :	real link position of the pendulum
K_s :	resultant physical stiffness around pivot
B :	real viscous coefficient around pivot
K_d :	desired spring constant of the impedance
B_d :	desired viscous coefficient of the impedance

1. The compliance controller with steerable equilibrium to accommodate the inclination varying slope;
2. The estimation of the terrain inclination based on the integration of sensory data from the inertial measurement unit (IMU), the kinematics of the robot, and the foot-ground contacts.

The compliance controller is based on an admittance control approach using the force/torque feedback in the feet to modify the COM position references for achieving the desired compliance and passivity. Compared to our previous study [9], the presented work here provides more rigorous formulation of the overall control principle, and significantly extends more experimental validations, including the implementation of walking in place on an inclination varying platform. The terrain inclination estimation algorithm is improved to be more generic for both standing and walking scenarios by combining the estimation from each foot depending on the support phases. All the control algorithms were validated on the lower-body prototype of the **COMpliant HuMANoid (COMAN)** robot.

The paper is organized as follows. Section 2 presents the compliance control using the passivity based admittance scheme, elaborates the principles of the terrain inclination estimation, and delineates the control framework. Section 3 is the experimental validations of the inclination estimation, the comparison study of the stabilization effects, and the stabilization of standing and walking on the slope with changing inclination. In Section 4, we discuss the limitations of the algorithms. We conclude the study and suggest future work in Section 5.

2 Control Principles

Fig. 1 shows the kinematic configuration and the allocation of stiff/compliant joints of the whole-body COMAN. The compliant joint is made of series elastic actuator (SEA). COMAN has 6 degrees of freedom (DOFs) in each leg, 3 DOFs in the waist, 4 DOFs in each arm,

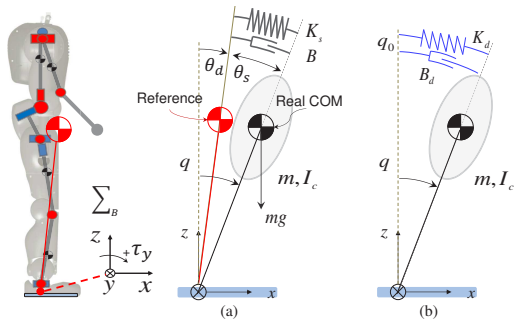


Fig. 2 Simplified model for admittance control (sagittal plane).

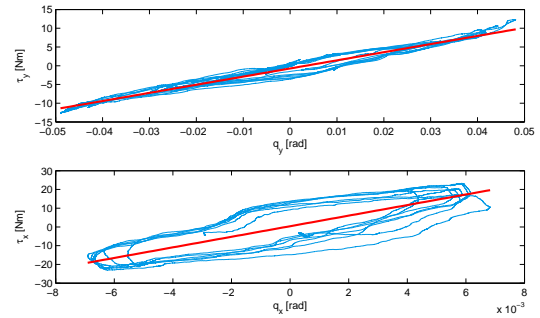
and 2 DOFs of a parallel mechanism in its neck. It is an upgrade version based on the compliant leg prototype in [22]. More technical details of the COMAN design can be found in [23]. The used parameters in the following formulation and figures are listed in Table 1.

2.1 Compliance based Stabilization Control

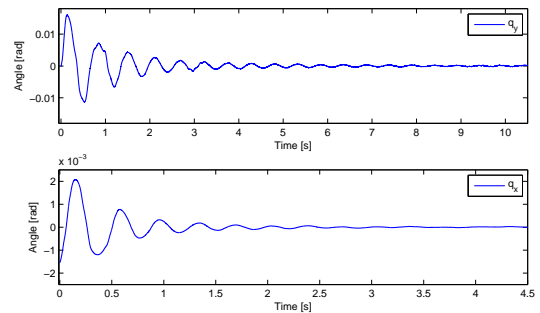
In the control formulation, the origin of reference frame \sum_B is at the midpoint of two horizontal projections of ankle joints. Note that \sum_B is a local frame virtually attached at the polygon of support formed by two feet. The robot is simplified as a single rigid body mounted on the top of an inverted pendulum with mass m and moment of inertia I_c around the COM, as shown in Fig. 2(a). When the robot stands on a changing slope, \sum_B moves together with the virtual polygon whereas a world coordinate \sum_W is constantly stationary. Let k_p and k_s be the stiffness at the COM level contributed by the PD gains from the motor controllers and the intrinsic joint elasticity respectively. Hence, the equivalent torsional stiffness K_s at the COM is $\frac{k_p k_s}{k_p + k_s}$ in \sum_B .

It shall be noted that the formulation here is done in the polar coordinate. Therefore, the rotational motion around x axis corresponds to translational displacement in the lateral plane, while the rotational motion around y axis corresponds to translational displacement in the sagittal plane, and vice versa.

Fig. 3(a) and Fig. 3(b) show the experimental identification of stiffness and damping respectively using least square fitting. The stiffness are 2822 N·m/rad and 217 N·m/rad around x and y axis respectively. The damping ratios are 0.27 and 0.072 around x and y axis respectively. Given the inertia and identified stiffness, these damping ratios correspond to the viscous coefficients of 47 N·m/(rad/s) and 3.5 N·m/(rad/s) around x and y axis respectively. These identified parameters were obtained at the neutral standing configuration



(a) Torque vs deflection profiles.



(b) Free damped oscillations.

Fig. 3 Identification of torsional stiffness and damping.

from the lower-body COMAN which was available during the time of conducting the experiments.

Denote by α the inclination of the terrain surface. The dynamics of this 1-DOF model in Fig. 2(a) is

$$I\ddot{q} = \tau_{ext} + \tau_g + K_s(\theta_d - q) + B(\dot{\theta}_d - \dot{q}), \quad (1)$$

where τ_{ext} is the resultant torque created by external forces or torques around the local frame \sum_B , and τ_g is the gravitational torque

$$\tau_g = mgl \sin(q + \alpha). \quad (2)$$

The advantage of formulating the controller in a polar coordinate is that the external disturbance as a wrench, namely force and torque, will appear in a unified term as the net torque τ_{ext} in reference frame \sum_B .

As shown in Fig. 2(b), the desired spring K_d and damping B_d are the property of interest to emulate, but inertia tensor of the robot is not influenced by our controller. In other words, the desired inertia is always the same as that of the physical system $I_d = I$, so the controller does not shape the inertia property.

Define by q_0 and \dot{q}_0 the position and the velocity of the desired equilibrium set-point of the pendulum. The dynamic equation of this desired system is

$$I\ddot{q} = \tau_{ext} + K_d(q_0 - q) + B_d(\dot{q}_0 - \dot{q}). \quad (3)$$

If the net torque exerted by the gravity and spring deflexion is equal to the desired torque defined by the virtual spring damper system such as

$$\tau_g + K_s(\theta_d - q) + B(\dot{\theta}_d - \dot{q}) = K_d(q_0 - q) + B_d(\dot{q}_0 - \dot{q}) \quad (4)$$

then these two systems appear to have the same dynamic response at the COM level.

Note that the term ' $K_s(\theta_d - q) + B(\dot{\theta}_d - \dot{q})$ ' in (4) implies the feasibility of controlling the torque by changing reference θ_d to satisfy (4) via active regulation of the spring deflexion.

Rearrange (4), we obtain the relation between the reference position θ_d based on the real COM position,

$$\theta_d = \frac{K_d}{K_s}q_0 + \frac{K_s - K_d}{K_s}q + \frac{B_d - B}{K_s}(\dot{q}_0 - \dot{q}) - \frac{\tau_g}{K_s}. \quad (5)$$

Denote by τ the applied torque in \sum_B ,

$$\begin{cases} \tau = -K_s\theta_s, \\ q = \theta_d + \theta_s. \end{cases} \quad (6)$$

So q and \dot{q} can be obtained as

$$\begin{cases} q = \theta_d - \frac{\tau}{K_s}, \\ \dot{q} = \dot{\theta}_d - \frac{\dot{\tau}}{K_s}. \end{cases} \quad (7)$$

Substitute (7) into (5), yields

$$\begin{aligned} \theta_d = & \frac{K_d}{K_s}q_0 + \frac{B_d - B}{K_s}\dot{q}_0 + \frac{K_s - K_d}{K_s}\theta_d - \frac{B_d - B}{K_s}\dot{\theta}_d \\ & - \frac{K_s - K_d}{K_s^2}\tau + \frac{B_d - B}{K_s^2}\dot{\tau} - \frac{\tau_g}{K_s}. \end{aligned} \quad (8)$$

The above is the formulation in a continuous time representation. In a discrete-time system, the desired angular velocity $\dot{\theta}_d$ can be substituted by the derivative of the ideal reference using the implicit Euler method

$$\dot{\theta}_d = \frac{\theta_d(i) - \theta_d(i-1)}{T}. \quad (9)$$

Substitute (9) into (8), the desired reference angle θ_d is derived in a discrete form, given the feedback $\tau(i)$ and the sampling time T at the i th control loop,

$$\theta_d(i) = \frac{T}{K_dT + B_d - B}A(i) + \frac{B_d - B}{K_dT + B_d - B}\theta_d(i-1), \quad (10)$$

where A is an intermediate term

$$\begin{aligned} A(i) = & K_dq_0(i) + (B_d - B)\dot{q}_0(i) + \frac{K_d - K_s}{K_s}\tau(i) \\ & + \frac{B_d - B}{K_s}\dot{\tau}(i) - \tau_g(i). \end{aligned} \quad (11)$$

For a rigid actuation with no physical compliance in the gear transmission, a variant of admittance formula can be obtained by setting $K_s \rightarrow \infty$ in (11), and the resulting A becomes

$$A(i) = K_dq_0(i) + (B_d - B)\dot{q}_0(i) - \tau(i) - \tau_g(i). \quad (12)$$

If the robot stands on a slope of inclination $\alpha(i)$, the gravity torque used in (11) and (12) is approximated by

$$\tau_g(i) = mgl \sin(\theta_d(i-1) - \frac{\tau(i)}{K_s} + \alpha(i)). \quad (13)$$

Equation (10) is the general equation to achieve the admittance control for a 1-DOF system. Equation (11) can be implemented for the system with intrinsic elasticity, whereas (12) is suitable for a classical actuation system with rigid transmission.

Our proposed admittance formula requires the force and torque sensor feedback from feet to compute the resultant torque created by the ground reaction forces. This forms the input of our admittance scheme which subsequently generates a modification of the reference position as an output that deviates from the desired set-point of equilibrium. Therefore, the reaction torque applied to the system is indirectly controlled by modulating the COM reference. In reality, the real system undoubtedly respects the physical causality of 'force→motion' for replicating the desired behavior of a spring-damper system, and the admittance controller functions as a way of rendering force and torque.

The level of compliance is adjusted by the desired stiffness, and the passivity is warranted by introducing sufficient active damping. As suggested by the identified damping ratios shown in Fig. 3(b), the real system is passive but under-damped. Hence, imposing additional controlled viscosity can effectively increase the damping ratio, and keep the system passive and stable.

2.2 Estimation of the Terrain Inclination

Without the visual perception of the environment, the physical foot-ground contact is the only potential means for a robot to perceive the terrain information in a similar manner to haptic exploration. The proprioception data computed from the measurement of IMU and the kinematics of the robot from joint encoders are combined together with the force/torque sensors in the feet to determine the terrain inclination.

In the literature, most balancing controllers assumed by default that the feet were perfectly aligned with the ground surface. However, this is not a generic scenario. Fig. 4 shows different contact cases to illustrate the relation between the inclination of the foot

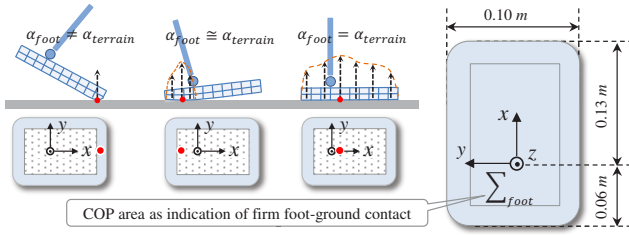


Fig. 4 Exploration of terrain inclination via foot-ground contact.

and the terrain. We find that it is critical to apply different control strategies depending on the contact phases in order to guarantee a stable control action, because stationary feet correspond to a fully actuated phase, whereas the tilting feet belong to the under-actuated phase. Hence, in general, the control law derived for one case does not apply to another.

The real feet of the robot are not ideally rigid. Fig. 4 illustrates unavoidable foot deformation under a considerable load during heel contact, particularly when the ground reaction forces act at the edge of the foot. Fig. 4 also shows a straightforward correlation of foot and terrain inclination, depending on the center of pressure (COP) location in the foot. We observe that when the COP resides at the narrow strip near the edge of the foot, the inclination of foot and terrain no longer coincides with each other due to the deformation.

Therefore, the foot is only a valid probe of the terrain inclination when it is loaded properly on the surface, hence logical judgments are necessary to be introduced into the terrain inclination estimation for classifying different foot-ground contacts. In the following formulation, let us define $\alpha_f^{l,r}$, $\alpha_t^{l,r}$ and $\hat{\alpha}_t$ as the direct inclination of the foot, the estimated inclinations of the foot and the terrain respectively. The superscripts l,r are used to denote the left and right foot respectively, and the subscripts f,t stand for foot and terrain.

The orientation of the feet with respect to the world frame are computed by the IMU measurement and the kinematics calculated from all joint encoders

$$R_f^{l,r} = R_{IMU} R_{l,r}, \quad (14)$$

where R_{IMU} is the orientation of the IMU computed from the pitch and roll angles, excluding the yaw angle which is the heading in the earth magnetic field; and $R_{l,r}$ are the left/right foot orientations with respect to the waist computed by the forward kinematics. The IMU sensor is mounted on the waist of the robot.

Let \mathbf{k}_f^l and \mathbf{k}_f^r be the unit vectors along z axis in the local frame of left/right foot $\Sigma_f^{l,r}$, these normal vectors with respect to the world frame are

$$\mathbf{k}_w^{l,r} = R_f^{l,r} \mathbf{k}_f^{l,r}. \quad (15)$$

The inclination $\alpha_{x,y}$ around x,y axis of each foot is

$$\begin{cases} \alpha_x^{l,r} = \text{atan2}(-(k_w^{l,r})_y, (k_w^{l,r})_z), \\ \alpha_y^{l,r} = \text{atan2}((k_w^{l,r})_x, (k_w^{l,r})_z). \end{cases} \quad (16)$$

To eliminate the incorrect estimations during the under-actuation phase, the estimated terrain inclination α_t of each foot is updated by the sampled inclination of the foot α_f only when the COP in the foot exists in a constrained region, as shown by the dotted area in Fig. 4, and the vertical ground reaction force F_z is greater than the threshold F_z^{min} . The reason is that under these conditions the bending deformation of the foot structure is negligible, hence the foot orientation can be considered the same as the ground orientation. Note that this concept is different from the conventional definition of the safety margin in the ZMP based walking control.

$$\begin{cases} \alpha_t(i) = \alpha_f(i), \text{ if } \mathbf{X} \cap \mathbf{Y} \cap \mathbf{F}, \\ \alpha_t(i) = \alpha_f(i-1), \text{ otherwise,} \end{cases} \quad (17)$$

where

$$\begin{cases} \mathbf{X} = \{x : x_{cop}^- \leq x_{cop} \leq x_{cop}^+\}, \\ \mathbf{Y} = \{y : y_{cop}^- \leq y_{cop} \leq y_{cop}^+\}, \\ \mathbf{F} = F_z > F_z^{min}. \end{cases} \quad (18)$$

These boundary limits of \mathbf{X} and \mathbf{Y} were experimentally identified for each foot in a straightforward manner. Take the x axis for example, we applied very static external force along the positive direction of x axis, and increased the force gradually until the rear edge of the foot lifted up with a visible clearance from the ground surface, e.g. 1-2 mm. The measured COP location was then considered as one boundary limit. The same procedure was repeated several times to obtain an average value, and was the same for other axial directions. These boundary values are: $x_{cop}^- = -0.03$ m, $x_{cop}^+ = 0.10$ m, $y_{cop}^- = -0.04$ m, $y_{cop}^+ = 0.04$ m.

The threshold of the force/torque sensor in foot was set as $F_z^{min} = 10N$ for keeping away from sensor noise and the non-zero readings while foot was in aerial phase. However, it should be noted that the measurable values of x_{cop} and y_{cop} were confined by the real physical dimension of the foot (Fig. 4), but not by the thresholds used in the inclination estimation (18).

The proposed logic condition $\mathbf{X} \cap \mathbf{Y} \cap \mathbf{F}$ suggests a firm foot placement such that $\alpha_t = \alpha_f$ is the most probable case. The estimation α_t holds its previous value, if $\mathbf{X} \cap \mathbf{Y} \cap \mathbf{F}$ is not satisfied. In other words, α_t relies on its history if no reliable detection is available. For instance, when feet tilt, the foot inclination should not be assigned to the estimation of terrain inclination, so in this case $\alpha_t \neq \alpha_f$.

By classifying the foot-ground contact into different situations as in (14) to (18), we obtain the terrain inclination estimation $\alpha_t^{l,r}$ from the left and right foot respectively. Then, depending on the foot support phases, i.e. left/right single support phase or double support phase, the overall estimation $\hat{\alpha}_t$ of the terrain inclination is updated based on the support phases determined by the vertical ground contact forces:

$$\begin{cases} \hat{\alpha}_t(i) = \alpha_t^l(i), & \text{if } F_z^l > F_z^{min} \wedge F_z^r < F_z^{min}, \\ \hat{\alpha}_t(i) = \alpha_t^r(i), & \text{if } F_z^r > F_z^{min} \wedge F_z^l < F_z^{min}, \\ \hat{\alpha}_t(i) = 0.5 \cdot (\alpha_t^l(i) + \alpha_t^r(i)), & \text{if } F_z^{l,r} > F_z^{min}, \\ \hat{\alpha}_t(i) = \hat{\alpha}_t(i-1), & \text{otherwise.} \end{cases} \quad (19)$$

In other words, when the left foot is in contact with the ground, i.e. $F_z^l > F_z^{min}$ and $F_z^r < F_z^{min}$, the overall terrain inclination $\hat{\alpha}_t$ is estimated from the left foot α_t^l , and vice versa. When both feet are in good contact with the ground, i.e. $F_z^{l,r} > F_z^{min}$, then $\hat{\alpha}_t$ is the average of the estimations from both feet.

It should be noted that this logical judgment introduces discontinuous values into $\hat{\alpha}_t$, when the foot-ground interaction is changing. Therefore, for each estimation, a first order low-pass filter is applied. Thus the high frequency component introduced by the discontinuity in $\hat{\alpha}_t$ is eliminated to obtain smoothly filtered estimation $\hat{\alpha}_t^{filter}$ without causing unstable oscillation of the equilibrium set-point in the compliance controller.

Compared to an over simplified approach where the inclination of terrain is regarded the same as that of the feet, where $\alpha_t(i) = \alpha_f(i)$ without the logic condition (18) to delineate different scenarios of foot-ground contact, our experimental comparison shows that our proposed algorithm of using $\hat{\alpha}_t^{filter}$ from (17), (18), and (19) was very useful to prevent false estimations of the terrain inclination, especially when there were slight deformations of feet due to the ground reaction forces acting on the edges of the feet, or during the under-actuation phases when feet were rotating around their edges. Moreover, the integration of compliance control, as it will be shown in Section 2.3, produced compliant and stable of foot-ground contact thus in turn warranted a better estimation for (19). This difference will be shown by the comparison study in Section 3.3, and can also be seen from the accompanying video.

2.3 Control Framework

Suppose the feet of the robot are firm on the terrain surface, namely the fully actuated phase, then balancing on the changing slope simply requires the equilibrium point in the admittance controller to move in the direction opposite to the foot inclination. Though in fact,

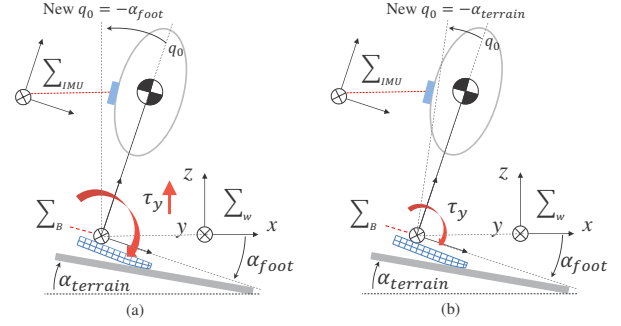


Fig. 5 Adaptation to inclined surface (a) wrong action, (b) correct action.

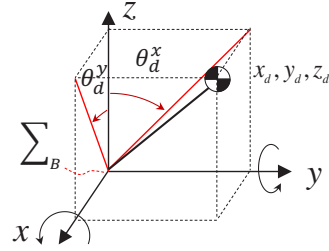


Fig. 6 Projection of planar motions to the spatial motion.

this is not always valid, as suggested in Fig. 5 where the foot and the floor surface are not aligned.

Once the feet rotate, the under-actuation phase emerges such that the torque around the edge is always zero. If the robot continues steering the equilibrium opposite to the foot inclination as in the fully actuated phase, then a larger torque will be produced, which in turn tilts the foot even more. Consequently, this increasing foot inclination will be sensed by the feedback loop, which misleads the controller to produce an even larger ankle torque, as shown by the red illustration of torque in Fig. 5(a). All these co-actions constantly inject more energy into the system with the similar effect of positive feedback. As a result, the system will be unstable once the under-actuation phase is triggered.

Our study showed that the correct control action to balance on an inclination varying slope was to adapt the equilibrium set-point only to the terrain inclination, as shown in Fig. 5(b), rather than the foot inclination. Hence, the estimation of terrain inclination $\hat{\alpha}_t^{filter}$ shall be used to update the set-point q_0 in (10) and (11). Therefore, during the under-actuation, the whole robot holds the same equilibrium point, behaves as a passive spring-damper system, and actively dissipates excessive energy until the feet conform back to the terrain surface. Hence, the passivity of the system is constantly guaranteed. Certainly, in this paper, we discuss only the cases where the disturbance is moderate and not large enough to completely tip over the robot.

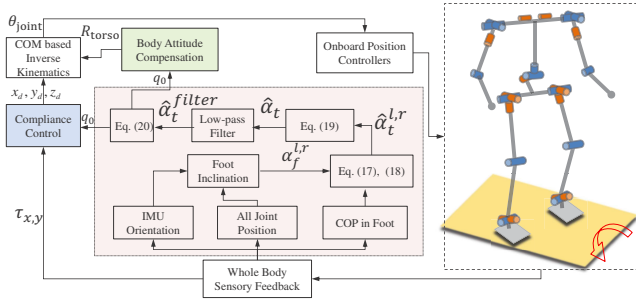


Fig. 7 Control framework for the stabilization on a slope with changing inclination.

The equilibrium point of the desired spring-damper system is updated with respect to the base frame \sum_B by

$$\mathbf{q}_0 = -\hat{\alpha}_t^{filter}, \quad (20)$$

as illustrated in Fig. 5(b). \mathbf{q}_0 is the 2D vector that contains the inclination in the sagittal and lateral planes, and is substituted into (11).

In \sum_B , denote by $\mathbf{a} = [0, 0, 1]^T$ the unit normal vector, and by \mathbf{b} the unit vector along the updated equilibrium point. The element of \mathbf{b} is calculated by

$$\begin{cases} b_z = \cos(\text{atan2}(\sqrt{(\tan q_{0,x})^2 + (\tan q_{0,y})^2}, 1)), \\ b_x = b_z \cdot \tan q_{0,y}, \\ b_y = b_z \cdot \tan(-q_{0,x}). \end{cases} \quad (21)$$

In \sum_B , according to the adjusted equilibrium, the orientation of the torso is compensated as

$$R_{torso} = R_{rodrigues}(\mathbf{n}, \varphi) \quad (22)$$

in order to keep the upper body in an upright posture for the steady state. The intermediate variables are

$$\begin{cases} \mathbf{n} = \frac{\mathbf{a} \times \mathbf{b}}{\|\mathbf{a} \times \mathbf{b}\|}, \\ \varphi = \text{acos}\left(\frac{\mathbf{a} \cdot \mathbf{b}}{\|\mathbf{a} \cdot \mathbf{b}\|}\right), \end{cases} \quad (23)$$

where \mathbf{n} is the unit vector around which the angular rotation of φ is performed, and $R_{rodrigues}$ is Rodrigues' rotation formula.

The tangential components of the resultant torque in \sum_B are computed by

$$\boldsymbol{\tau}_{x,y} = (\boldsymbol{\tau}_l + \boldsymbol{\tau}_r + \mathbf{r}_{f_l} \times \mathbf{f}_l + \mathbf{r}_{f_r} \times \mathbf{f}_r)_{x,y}, \quad (24)$$

where $\boldsymbol{\tau}_l$, \mathbf{f}_l and $\boldsymbol{\tau}_r$, \mathbf{f}_r are the force and torque vectors measured by the F/T sensor in left and right foot respectively, and \mathbf{r}_{f_l} and \mathbf{r}_{f_r} are the position vectors from the origin of \sum_B to the origins of the F/T sensor in the left and right foot respectively.

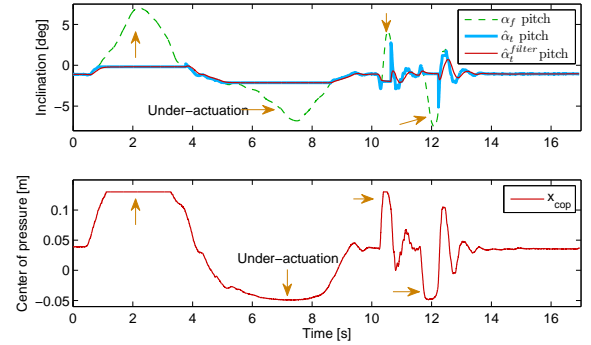


Fig. 8 Experiment I: sagittal inclination estimation on the flat ground.

The 1-DOF admittance controller is applied in a decoupled manner around the x, y axis separately in the spherical coordinate as shown in Fig. 6, since it is derived in a rotational form. The feedback variables from (20) and (24) are substituted into (10) to obtain desired rotational reference position θ_d^x and θ_d^y , where the superscripts x, y indicate that the variables are defined around the x, y axes. Then, the corresponding spatial COM reference position in the Cartesian coordinate is computed as

$$\begin{cases} z_d = l \cdot \cos(\text{atan2}(\sqrt{(\tan \theta_d^x)^2 + (\tan \theta_d^y)^2}, 1)), \\ x_d = z_d \cdot \tan \theta_d^y, \\ y_d = z_d \cdot \tan(-\theta_d^x). \end{cases} \quad (25)$$

To balance in the standing posture, the desired position and orientation of the feet are constant in \sum_B . The desired parameters, such as the torso orientation from (22), the COM position from (25), the constant position and orientation of the feet are the inputs of the COM based inverse kinematics. Details of the COM based inverse kinematics can be found in [8]. The outputs are the joint position references for the on-board controllers embedded in the robot.

Fig. 7 shows the control framework. The central module is the terrain inclination detection that estimates the inclination of the slope and modulates the equilibrium. The updated equilibrium is used in the stabilization module for keeping the COM's projection at the origin of the support polygon, and also in the attitude compensation for keeping the torso upright.

3 Experiments

To evaluate the proposed control framework, a series of experiments were designed to validate the effectiveness in an increasing complexity. The experimental videos are available in the supplementary materials. The experiments are as follows:

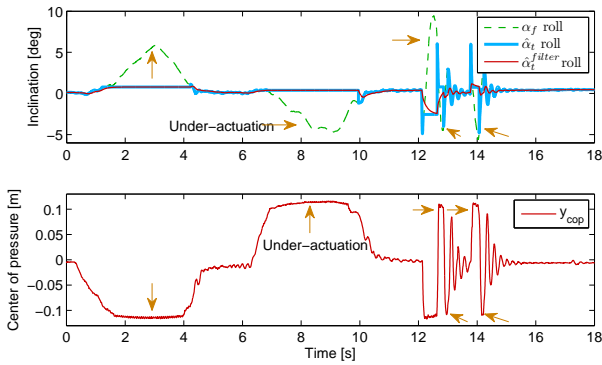


Fig. 9 Experiment I: lateral inclination estimation on the flat ground.

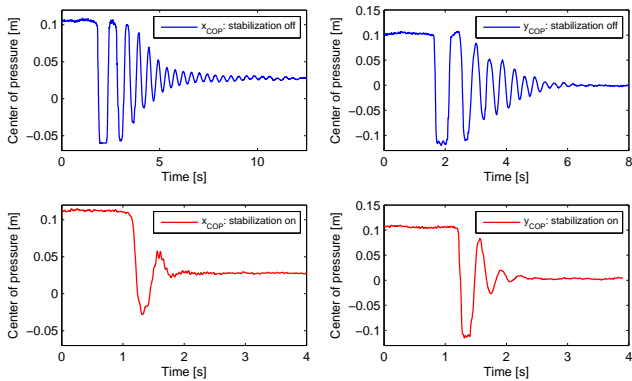


Fig. 10 Experiment II: COP responses without/with stabilization after a constant push.

1. Validation of terrain inclination estimation involving the under-actuation phase;
2. Comparison study of disturbance rejection without and then with the stabilization control;
3. Comparison study of stabilization against an impact without and then with the conditional logic judgment in the terrain inclination estimation;
4. Standing stabilization on the slope with changing inclination in both sagittal and lateral planes;
5. Walking in place on the slope with changing inclination in sagittal and lateral plane respectively.

The control parameters used for the experiments are as follows. For standing stabilization, the cutoff frequency of the low-pass filters was 5 Hz for filtering $\hat{\alpha}_t$; the desired stiffness and viscous coefficient were $K_d^y = 110$ N·m/rad, $B_d^y = 50$ N·m/(rad/s) around the y axis (sagittal plane), and $K_d^x = 225$ N·m/rad, $B_d^x = 135$ N·m/(rad/s) around the x axis (lateral plane). For walking in place, the cutoff frequency for the lateral inclination was reduced to 2 Hz due to the fluctuation of estimated inclination during the change of support foot; the desired stiffness and viscous coefficient were $K_d^y = 110$ N·m/rad, $B_d^y = 80$ N·m/(rad/s) around the y

axis (sagittal plane), and $K_d^x = 800$ N·m/rad, $B_d^x = 400$ N·m/(rad/s) around the x axis (lateral plane).

3.1 Experiment I

The first experiment validated the accuracy of the terrain inclination estimation. The robot was placed on a flat ground so the real terrain inclination shall be close to zero. Constant and impulsive force disturbances were applied in the sagittal and lateral plane respectively. During the constant disturbance, the robot was pushed until the feet tilted more than 5° and the corresponding COP moved to the edge of support foot, as marked by the under-actuation phases in Fig. 8 and Fig. 9.

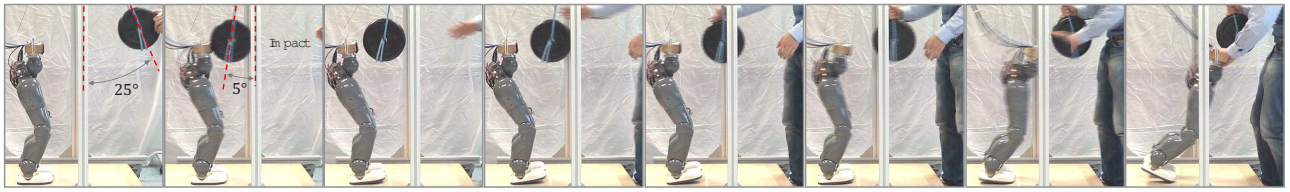
Both the inclination estimation and the COP measurement are included in Fig. 8 and Fig. 9 to show the change of $\hat{\alpha}_t^{filter}$ related with the COP. When the COP moved out of the threshold defined in (18), the feet were no longer in firm contact with the ground. Therefore, the estimation $\hat{\alpha}_t^{filter}$ was no longer updated, and differed from the direct foot inclination α_f . We found that (17) was particularly effective, because during the under-actuation using low-pass filtering could not resolve the problem of a false estimation. On the contrary, the conditional judgments proposed in (18) retained the reasonable past estimation, discarded the improbable value when feet were not aligned on the terrain surface, and continued updating once (18) was satisfied.

The discontinuity introduced by the discrete update in (17) can be smoothed by low-pass filters, the data in Fig. 8 and Fig. 9 show the smoothly filtered estimations. For the experiments done on the lab floor, the average estimation of the sagittal inclination was -1.2° with standard deviation of 0.69° , and the average estimation of the lateral inclination was -0.66° with standard deviation of 0.71° .

3.2 Experiment II

The second type of experiments examined the effectiveness of the compliance based stabilization. In the comparison study, the robot was pushed statically by a constant force until the COM was placed at approximately 0.1 m, then the robot was released and fell back freely. The steady state equilibriums for the x, y directions were 0.03 m and 0 m respectively.

The top figures in Fig. 10 show the oscillations of the COP after the free landing. Without the stabilization, the robot rocked back and forth, left and right due to the ground impacts. The oscillation motion around the edge of the feet can be indicated by the saturated COP measurements at the maximum values. These undesired



(a) Without the logic based judgment in the estimation of the terrain inclination.



(b) With the logic based judgment in the estimation of the terrain inclination.

Fig. 11 Experiment III: comparison of the terrain inclination estimation for stabilizing against an impact (time spaced 1/6 s since 2nd snapshot).

responses lasted for more than 4 – 6 s in sagittal and lateral planes. In contrast, these impacts were properly absorbed and damped out within 1 s in both cases with the active stabilization enabled, as shown by the bottom figures in Fig. 10.

3.3 Experiment III

The comparison study here used an impact test to validate the effectiveness of the conditional judgment (17) and (18) in the terrain inclination estimation. A 5 kg weight was suspended with a pendulum length of 0.75 m. The initial angle of launching the weight was 25° , the final angle at the instant of impact was 5° . Therefore, the velocity of the weight converted from the potential energy at the instant of impact was 1.15 m/s. Both impact instants are aligned at the 0.5 s and marked by vertical lines in Fig. 12.

Fig. 11(a) shows the snapshots of the robot's response without the logic-based terrain estimation, and Fig. 12(a) shows the corresponding COP response and the inclination estimation. Without the conditional judgment, $\hat{\alpha}_t = \alpha_f$ was always assumed, so that the robot misinterpreted the foot inclination as the terrain inclination during the under-actuation phase. On this false assumption, the robot tilted up feet to adapt to a fictitious slope as if it stood on an inclined surface, as shown by the 5th snapshot in Fig. 11(a). In Fig. 12(a), during 0.6 – 1.4 s, the COP was at the edge of rear feet, the false inclination estimation was non-zero whereas the real ground was actually flat. Therefore, the over-tilting of the feet elongated the under-actuation phase and the robot overthrew itself while falling back after 1.4 s, as shown by the forward falling in Fig. 11(a) and

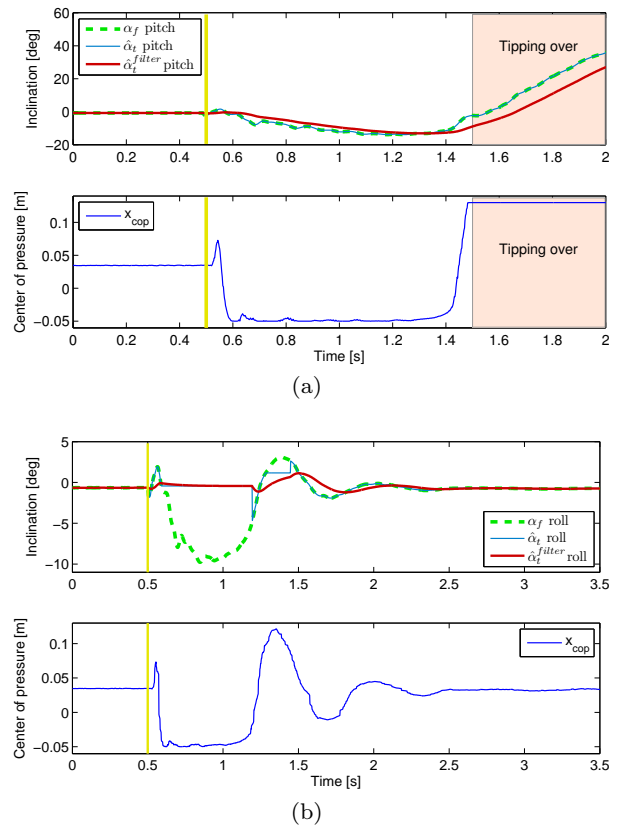
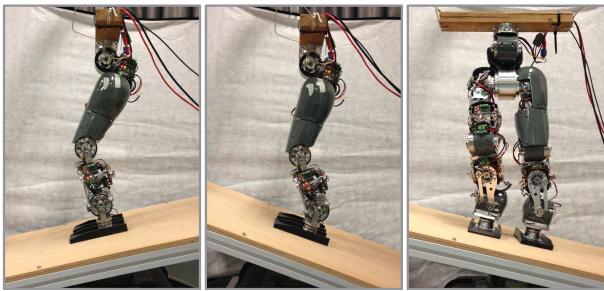


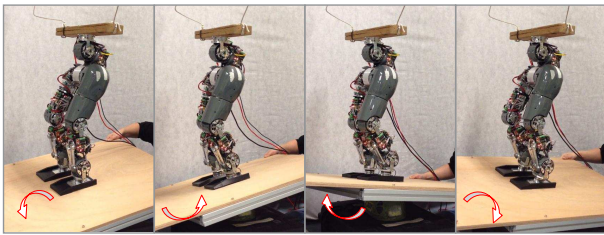
Fig. 12 Experiment III: estimation of foot/ground inclination and the COP response without (a) and then with (b) the logic-based terrain estimation.

the drastic shift of the COP from the rear edge to the frontal edge of the feet in Fig. 12(a).

In contrast, Fig. 11(b) shows a stable reaction in response to the same impact. When the feet were rotating around the rear edge as indicated by the mini-



(a) Adapting to an inclined slope in the sagittal and lateral plane respectively.



(b) Balancing on a slope with changing inclination in both sagittal and lateral planes.

Fig. 13 Experiment IV: balancing on an inclination varying slope.

imum COP readings in Fig. 12(b) during 0.6–1.2 s, the logic-based terrain estimation ensured that the robot kept the most recent and reliable estimation of terrain inclination which was almost zero during this under-actuation phase. In this case, the whole system with the desired stiffness K_d and damping B_d guaranteed the passivity property by keeping the same equilibrium set-point in the admittance controller and by constantly dissipating the excessive energy delivered from the impact. Introducing the proposed conditional judgment in terrain estimation was straightforward and effective to prevent the feet from over-tilting, so the robot could regain full-actuation phase as soon as the feet were back in firm contact with the ground.

3.4 Experiment IV

The 4th experiment was a balancing task on a platform with the sagittal and lateral inclination disturbances. Fig. 13(a) qualitatively shows how the robot adapts to the inclined surface in the sagittal and lateral plane separately, and Fig. 13(b) displays the balancing performance on the platform with inclination disturbances in both sagittal and lateral planes.

The terrain inclination had an estimated amplitude of 5° around x axis, and of 8° around y axis from the estimation algorithm, as shown by the top figure in Fig. 14. The control algorithms allowed the robot to adapt

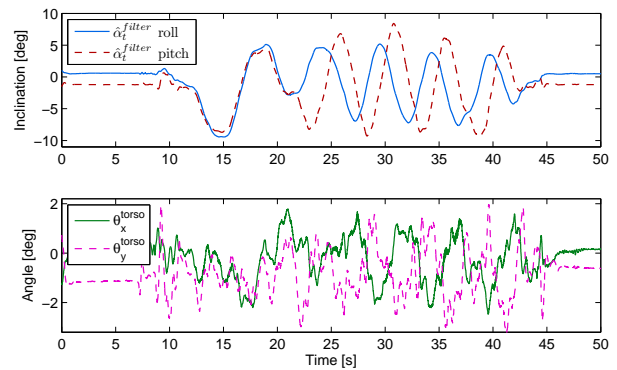


Fig. 14 Experiment IV: inclination estimation and torso orientation during inclination disturbance in both sagittal and lateral planes.

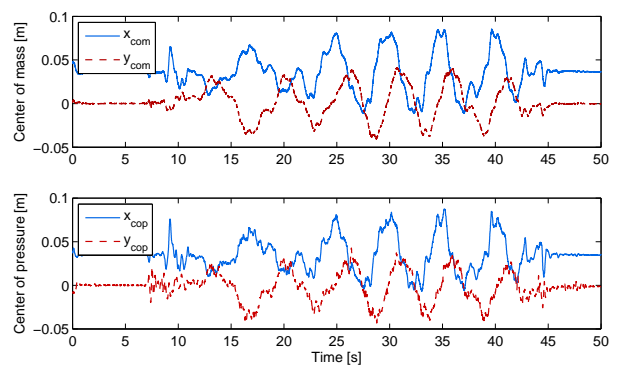


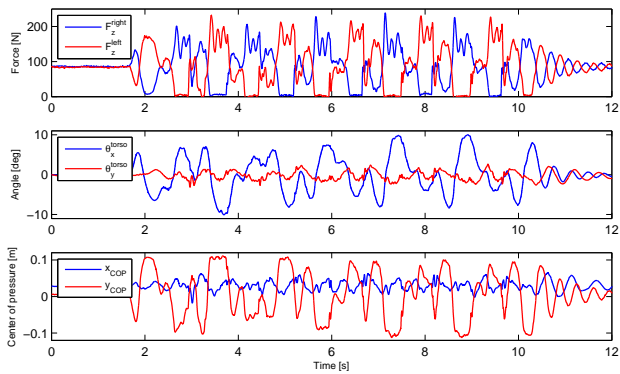
Fig. 15 Experiment IV: responses of COM and COP during inclination disturbance in both sagittal and lateral planes.

to the inclined surface and to maintain the torso upright. The orientation of the torso had variations within approximately 2° , as shown by the bottom figure in Fig. 14. Unfortunately, our control system was not equipped with an additional IMU for measuring the real orientation of the platform for the comparison with the estimation. However, the results were reasonable since the first experiment also served as benchmarking for the accuracy of the estimation.

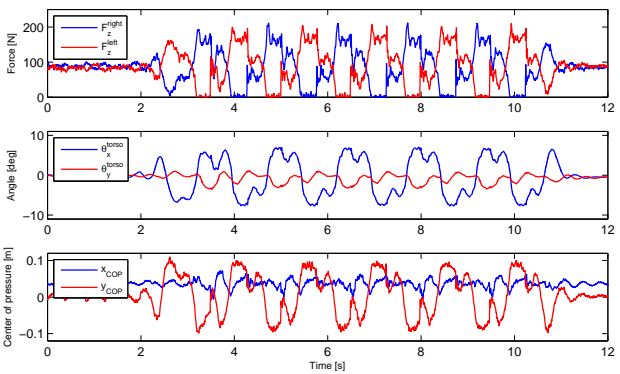
Fig. 15 shows the responses of COM and COP during these inclination disturbances. The horizontal projection of COM was always within the size of the support polygon formed by two feet. Without the adaptation algorithm, the robot was not able to stand on the changing slope because the horizontal projection of COM would inevitably go out of the support region even before the inclination reached the amplitude of 8° around y axis during these trials.

3.5 Experiment V

In addition to the standing stabilization, a preliminary investigation was conducted on the implementation of



(a) Walking in place without the stabilization.

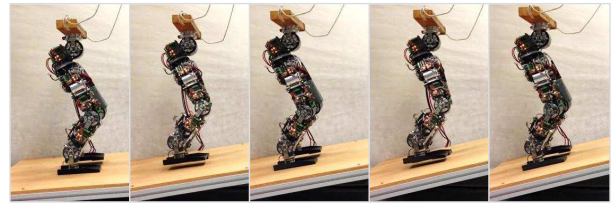


(b) Walking in place with the stabilization.

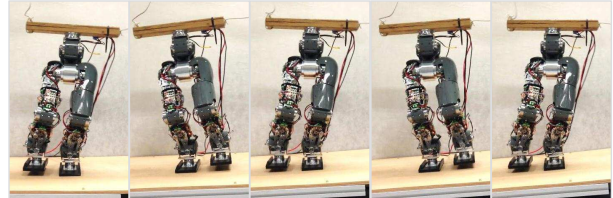
Fig. 16 Experiment V: comparison study of the stabilization effect during walking.

the proposed stabilizer for walking. The applied walking pattern was generated based on the COM state regulation and more details can be referenced in [10]. Walking in place was chosen here because two feet would only change the vertical position but keep the same horizontal position, thus a fixed coordinate \sum_B in our formulation can still be used as an inertia frame which was always in the center of the projections of two ankle joints. However, for generic walking gaits, the stabilizer should be formulated based on an inertia frame attached in each support polygon which switches discretely from step to step. Therefore, a generalization of the proposed stabilization for generic walking is fairly complicated. In the scope of this paper, we leave the sophisticated reformulation of the stabilization for generic walking as a future work, and concentrate on the particular setup of walking in place as an initial study.

The walking pattern generated desired COM and feet trajectories. The equilibrium point was adjusted according to the terrain inclination estimation, and the resultant torque with respect to \sum_B was computed by the F/T sensor feedback and foot position vectors as in (24). The output of the admittance controller was



(a) Sagittal inclination disturbance.



(b) Lateral inclination disturbance.

Fig. 17 Experiment V: walking in place with sagittal and lateral inclination disturbance separately.

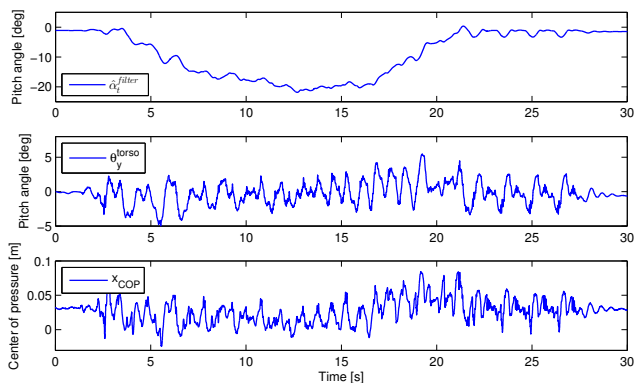
superimposed with the original COM trajectory to form a new COM reference. The new COM reference and the original feet trajectory were the inputs for the inverse kinematics to generate joint position references.

Fig. 16 shows the ground reaction forces, the torso orientation, and the COP measurements without and then with the stabilization during walking on the flat lab floor. The comparative study suggests that the stabilization particularly decreased the oscillation of the vertical ground reaction forces. Consequently, this reduction of undesired contact forces resulted in more repetitive patterns of the body attitude as well as the COP during the cyclic state of walking.

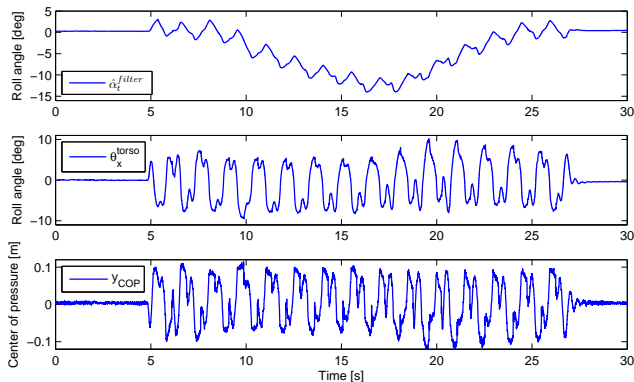
Fig. 17(a) and Fig. 18(a) show the snapshots and data of walking in place on a platform with changing inclination in the sagittal plane. The inclination of the platform had maximum change of -20° , the pitch angle of the torso orientation was within $\pm 5^\circ$ deviation, and the COP variation in the x axis of the support polygon was between -0.02 m and 0.08 m.

Fig. 17(b) and Fig. 18(b) show the snapshots and data of walking in place on a platform with changing inclination in the lateral plane. The platform's inclination had maximum change about -15° , the roll angle of the torso orientation was within $\pm 10^\circ$ deviation, and the COP in the y axis of the support polygon varied between two feet approximately within ± 0.1 m.

It should be noted that the estimation of terrain inclination in the sagittal plane was more desirable than that of the lateral plane. As shown in Fig. 4, each foot is 19 cm long and 10 cm wide, so the dimension of the foot along the x axis is much larger than that along the y axis. Therefore, the larger size of the foot in the sagittal plane permits more allowable time of firm contact



(a) Sagittal inclination disturbance.



(b) Lateral inclination disturbance.

Fig. 18 Experiment V: terrain inclination estimation, torso orientation, and COP response under the sagittal and lateral inclination disturbance respectively.

for each support foot to detect the terrain inclination. On the contrary, the foot has much smaller area of contact in the lateral plane, thus has more possibilities of having longer under-actuation phase during which the updating of terrain estimation is suspended.

This limitation introduced an undesired fluctuation of $\hat{\alpha}_t^{filter}$ into the regulation of the equilibrium set-point in the stabilization module, thus the torso orientation had more deviation than that of the sagittal scenario, as intuitively shown by Fig. 17(b) as well. This oscillation could possibly be reduced by further lowering the cut-off frequency for $\hat{\alpha}_t^{filter}$, however, this would also in turn trade off the response rate to the inclination variation. This limitation also suggests the development of feedback controllers based on the IMU for improving the dynamical performance of the torso attitude control as part of the future work.

4 Discussion

The proposed stabilization demonstrates the success in maintaining balance of a humanoid robot during standing and walking in place on a slope with changing inclination. The control algorithms are formulated based on a simplified model that captures the major dynamics of the real system, and demonstrate the effectiveness by the feedback control based stabilization.

The simplified model considers the entire robot as a rigid body in the local reference frame attached to the support polygon for implementing the 1-DOF resolution at the COM level, therefore, two feet are always parallel to form a planar polygon of support. Despite the robot as a whole can adapt to an inclined surface, the bottleneck is that each foot may not always conform with the contact surface in general. Hence, it could be interesting to investigate an improvement of modeling the compliance control for each foot or leg separately for the adaptation to more complex and rugged terrains.

The proposed terrain inclination estimation is based on the foot-ground contact and needs a surface or an area of contact. This means that if the contact region reduces to a line or a point, then the terrain inclination is no longer detectable. This is true during the under-actuation phase when the foot rotates. During this period, there is no physical means to detect the inclination if the terrain surface continues to change, for example, a moving rock.

In light of this limitation, therefore, the visual perception could be very useful in this case to perceive the change of inclination during under-actuation phases. Hence, the integration of visual perception with our proposed algorithm will produce a more robust terrain estimation, and thus permit a more versatile walking in complex terrains with soft surface or movable support.

5 Conclusion and Future Work

We proposed an admittance controller to achieve compliant and passive stabilization for humanoid robots. By integrating with the proposed terrain estimation algorithm, the posture stabilization was further extended to the adaptation to the slope with changing inclination. The feasibility of this control framework was demonstrated by the successful implementation on the compliant humanoid COMAN with different experimental trials in this paper.

A number of designed experiments demonstrated that the robot could adapt to the inclined surface with stabilized torso attitude in both sagittal and lateral planes. The logic-based terrain estimation algorithm exploited the foot-ground contact as a viable means to de-

tect the terrain inclination, and was effective to exclude false estimations during the under-actuation phase. A particular gait, i.e. walking on the spot, was selected for a further validation because it required no complication of modifying the proposed stabilization. The results of stabilization during walking on the spot suggested that the stabilizer reduced the ground impact and enabled the robot to walk in an inclination varying platform.

Our future work will focus on the improvement of the compliance control for each foot and leg separately, and the integration of visual feedback with our proposed method for a better estimation of the terrain inclination. Finally, with these future works, we will develop a more generic stabilization framework which is compatible with the bipedal walking control towards the agile locomotion of humanoid robots in complex and challenging real world environments.

Acknowledgments

This work is supported by FP7 European projects AMARSi (ICT-248311) and WALK-MAN (ICT-2013-10). We also acknowledge Phil E. Hudson for his generous help of the English corrections in this paper.

References

- Albu-Schaffer, A., Ott, C., Hirzinger, G.: A passivity based cartesian impedance controller for flexible joint robots-part II: Full state feedback, impedance design and experiments. In: IEEE International Conference on Robotics and Automation, vol. 3, pp. 2666–2672 (2004)
- Hashimoto, K., Sugahara, Y., Kawase, M., Ohta, A., Tanaka, C., Hayashi, A., Endo, N., Sawato, T., Lim, H., Takanashi, A.: Landing pattern modification method with predictive attitude and compliance control to deal with uneven terrain. In: IEEE/RSJ International Conference on Intelligent Robots and Systems, pp. 1755–1760 (2006)
- Hogan, N.: Stable execution of contact tasks using impedance control. In: IEEE International Conference on Robotics and Automation, vol. 4, pp. 1047–1054 (1987)
- Hyon, S., Cheng, G.: Passivity-based full-body force control for humanoids and application to dynamic balancing and locomotion. In: IEEE/RSJ International Conference on Intelligent Robots and Systems, pp. 4915–4922 (2006)
- Hyon, S., Hale, J., Cheng, G.: Full-body compliant human-humanoid interaction: Balancing in the presence of unknown external forces. IEEE Transactions on Robotics **23**(5), 884–898 (2007)
- Kim, J., Park, I., Oh, J.: Walking control algorithm of biped humanoid robot on uneven and inclined floor. Journal of Intelligent & Robotic Systems **48**(4), 457–484 (2007)
- Koolen, T., De Boer, T., Rebula, J., Goswami, A., Pratt, J.: Capturability-based analysis and control of legged locomotion, part 1: Theory and application to three simple gait models. The International Journal of Robotics Research **31**(9), 1094–1113 (2012)
- Li, Z., Tsagarakis, N., Caldwell, D.G.: A passivity based admittance control for stabilizing the compliant humanoid COMAN. In: IEEE-RAS International Conference on Humanoid Robots, pp. 44–49. Osaka, Japan (2012)
- Li, Z., Tsagarakis, N.G., Caldwell, D.G.: Stabilizing humanoids on slopes using terrain inclination estimation. In: 2013 IEEE/RSJ International Conference on Intelligent Robots and Systems (IROS), pp. 4124–4129 (2013)
- Li, Z., Tsagarakis, N.G., Caldwell, D.G.: Walking pattern generation for a humanoid robot with compliant joints. Autonomous Robots (2013)
- Nashner, L.M., McCollum, G.: The organization of human postural movements: a formal basis and experimental synthesis. Behavioral and brain sciences **8**(01), 135–150 (1985)
- Nenchev, D.N., Nishio, A.: Ankle and hip strategies for balance recovery of a biped subjected to an impact. Robotica **26**(5), 643–653 (2008)
- Ott, C., Albu-Schaffer, A., Kugi, A., Stamigioli, S., Hirzinger, G.: A passivity based cartesian impedance controller for flexible joint robots-part I: Torque feedback and gravity compensation. In: IEEE International Conference on Robotics and Automation, vol. 3, pp. 2659–2665 (2004)
- Ott, C., Baumgartner, C., Mayr, J., Fuchs, M., Burger, R., Lee, D., Eiberger, O., Albu-Schaffer, A., Grebenstein, M., Hirzinger, G.: Development of a biped robot with torque controlled joints. In: 10th IEEE-RAS International Conference on Humanoid Robots, pp. 167–173 (2010)
- Ott, C., Roa, M., Hirzinger, G.: Posture and balance control for biped robots based on contact force optimization. In: 11th IEEE-RAS International Conference on Humanoid Robots, pp. 26–33. Bled, Slovenia (2011)
- Pratt, J., Koolen, T., De Boer, T., Rebula, J., Cotton, S., Carff, J., Johnson, M., Neuhaus, P.: Capturability-based analysis and control of legged locomotion, part 2: Application to m2v2, a lower-body humanoid. The International Journal of Robotics Research **31**(10), 1117–1133 (2012)
- Runge, C., Shupert, C., Horak, F., Zajac, F.: Ankle and hip postural strategies defined by joint torques. Gait & Posture **10**(2), 161–170 (1999)
- Stephens, B.: Integral control of humanoid balance. In: IEEE/RSJ International Conference on Intelligent Robots and Systems, pp. 4020–4027 (2007)
- Stephens, B., Atkeson, C.: Dynamic balance force control for compliant humanoid robots. In: IEEE/RSJ International Conference on Intelligent Robots and Systems, pp. 1248–1255 (2010)
- Stephens, B., Atkeson, C.: Push recovery by stepping for humanoid robots with force controlled joints. In: 10th IEEE-RAS International Conference on Humanoid Robots (Humanoids), pp. 52–59 (2010)
- Sugahara, Y., Mikuriya, Y., Hashimoto, K., Hosobata, T., Sunazuka, H., Kawase, M., Lim, H., Takanashi, A.: Walking control method of biped locomotors on inclined plane. In: IEEE International Conference on Robotics and Automation, pp. 1977–1982 (2005)
- Tsagarakis, N., Li, Z., Saglia, J.A., Caldwell, D.G.: The design of the lower body of the compliant humanoid robot ‘cCub’. In: IEEE International Conference on Robotics and Automation, pp. 2035–2040. Shanghai, China (2011)
- Tsagarakis, N., Morfey, S., Medrano-Cerda, G., Li, Z., Caldwell, D.: Compliant humanoid coman: Optimal joint stiffness tuning for modal frequency control. In: IEEE

International Conference on Robotics and Automation
(ICRA), pp. 665–670 (2013)